

bradscholars

Controlled delivery of ciprofloxacin using zirconium-based MOFs and poly-caprolactone composites

Item Type	Article
Authors	Aden, S.F.;Mahmoud, L.A.M.;Ivanovska, E.H.;Terry, L.R.;Ting, V.P.;Katsikogianni, Maria;Nayak, Sanjit
Citation	Aden SF, Mahmoud LAM, Ivanovska EH et al (2023) Controlled delivery of ciprofloxacin using zirconium-based MOFs and poly-caprolactone composites. Journal of Drug Delivery Science and Technology. 88: 104894.
DOI	https://doi.org/10.1016/j.jddst.2023.104894
Rights	© 2023 The Authors. Published by Elsevier B.V. This is an open access article under the CC BY license (http://creativecommons.org/licenses/by/4.0/).
Download date	2026-06-10 06:50:12
Link to Item	http://hdl.handle.net/10454/20163



Controlled delivery of ciprofloxacin using zirconium-based MOFs and poly-caprolactone composites

Saynab F. Aden^{a,1}, Lila A.M. Mahmoud^{a,b,1}, Evdokiya H. Ivanovska^a, Lui R. Terry^c, Valeska P. Ting^{c,d}, Maria G. Katsikogianni^a, Sanjit Nayak^{a,*}

^a School of Chemistry and Biosciences, University of Bradford, Bradford, BD7 1DP, United Kingdom

^b School of Pharmacy, Al-Zaytoonah University of Jordan, Amman 11733, Jordan

^c Bristol Composites Institute, Department of Mechanical Engineering, University of Bristol, BS8 1TR, United Kingdom

^d Research School of Chemistry & College of Engineering, Computing and Cybernetics, The Australian National University, ACT 2600, Australia

ARTICLE INFO

Keywords:

Composites
Biodegradable
Antimicrobial
MOFs
Drug delivery

ABSTRACT

With antimicrobial resistance (AMR) increasing at an alarming rate, there is a need to develop better antibiotic delivery platforms at the point of need, to reduce over-exposure to antibiotics that are delivered systemically. Recent studies have suggested the use of metal-organic frameworks (MOFs) as potential vehicles for controlled and efficient delivery of various active pharmaceutical ingredients (APIs). Development of MOF-polymer composite materials can assist in the development of medical devices that can deliver APIs to local sites in a targeted approach. This study reports the encapsulation of a widely used antibiotic - ciprofloxacin (CIP) - into two Zr-based MOFs (UiO-66 and UiO-66-NH₂) and their subsequent integration into a biodegradable polymer; poly-caprolactone (PCL), via solvent casting, to obtain a PCL-MOF composite membrane. The MOFs and PCL-MOF composites were characterised by Fourier-transformed infrared (FT-IR) spectroscopy, powder X-ray diffraction (PXRD), thermogravimetric analysis (TGA) and scanning electron microscopy (SEM). The results demonstrated that the structural integrity of the pristine MOFs was maintained after drug loading and incorporation into the PCL membranes. The ciprofloxacin release was studied using ultraviolet-visible (UV-Vis) spectroscopy, and the results showed that the PCL-MOF composites had a more controlled drug release profile compared to the MOF alone, when monitored for seven days in phosphate buffered saline (PBS) and accelerated ageing (AA) release media. In addition, release studies showed pH-dependence with faster release of ciprofloxacin at both acidic and basic conditions. Antimicrobial assay showed excellent efficacy for both CIP-loaded MOFs and their PCL composites against *S. aureus* and *E. coli*, a Gram-negative and Gram-positive bacterium, respectively, with inhibition zone as high as >50 mm against *E. coli* for UiO-66-NH₂-CIP, indicating their potential applications in purpose-specific medical devices.

1. Introduction

According to the World Health Organisation (WHO), antimicrobial resistance (AMR) is one of the top ten critical issues faced by humanity [1], and it is predicted that it will approximately cause 10 million annual deaths worldwide by 2050 [2]. AMR is defined as the ability of microorganisms to resist the effect antimicrobial agents have on them, through various adaptive mechanisms [3]. In the past decades, numerous generations of antimicrobial drug classes were developed to combat this issue, including penicillin, cephalosporins and quinolones

[4]. However, due to their excessive and improper use and over-prescription [5], drug-resistant strains of bacteria, fungi, and viruses have emerged [6–8]. Methicillin-resistant *Staphylococcus aureus* (MRSA) is such an example, with it being a strain of *S. aureus* that has developed resistance against all classes of β -lactam antibiotics and other antibiotic classes [9]. It is thought that MRSA emerged because of the overuse of antimicrobial agents in hospital settings, resulting in an alarmingly high prevalence in hospitals worldwide and in severe economic burden on many countries. According to the US Centers for Disease Control and Prevention (CDC), the annual cost of fighting AMR in

* Corresponding author.

E-mail address: s.nayak@bradford.ac.uk (S. Nayak).

¹ These authors contributed equally to this work.

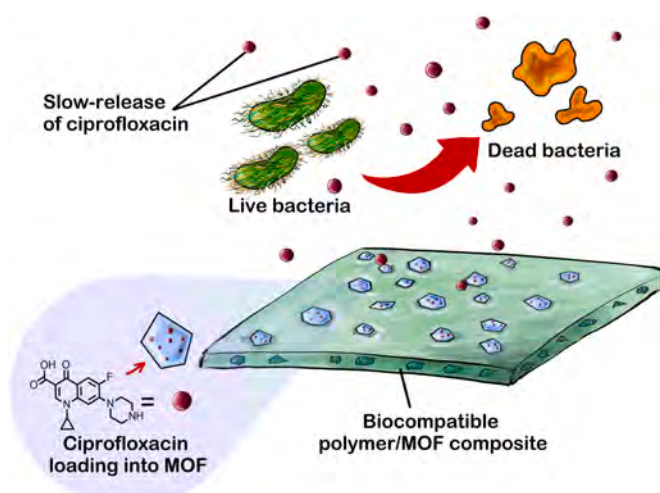
the US is \$55 billion, while in Europe, AMR infections cost € 1.5 billion annually in healthcare related costs and lost productivity [10].

Controlled and targeted delivery of antimicrobial drugs is a viable approach to reduce the development of AMR. Various systems, like liposomes [11], and other organic porous materials, including polymeric microsponges [12], are being studied for efficient and targeted delivery of antimicrobial drugs. Drug formulations towards enhanced and extended delivery can potentially assist in combating antimicrobial resistance via maintaining antibiotic concentrations above the minimum inhibitory concentration (MIC), in addition to maximising its therapeutic effect over the right amount of time [13]. However, these organic polymeric carriers retain low loading capacities, because of their comparatively low surface area, and their relatively poor stability. On the other hand, Metal-Organic Frameworks (MOFs) are coordination networks comprised of organic ligands that form potential voids [14]. Due to their customisable structure with varying metal ions and linkers, numerous MOFs have been developed in recent years [15]. Taking advantage of their ultra-high surface area, MOFs are studied widely for their potential applications in gas storage [16], catalysis [17], agricultural [18], and biomedical fields [19], due to their exceptionally high loading capacity and controlled release potential. Many studies on using MOFs as drug carriers have demonstrated excellent drug loading efficiencies, reaching almost 100% by weight [20].

Multiple studies have explored MOFs as delivery vehicle for anticancer agents like 5-fluorouracil and methotrexate [21,22]. In addition, the biocompatibility of several MOFs has been established via in vivo and in vitro studies [23], making these materials an attractive porous vehicle for controlled drug delivery, pharmaceutical formulations, and biomedical applications [24].

The antimicrobial action of MOFs can be attributed to multiple factors. For example, MOFs can act as a reservoir for slow release of loaded antimicrobial drug molecules, or their slow degradation can release the metal ions and organic linkers which can also have antimicrobial effects. Sometime the antimicrobial effect is enhanced by production of reactive oxygen species (ROS) triggered by external stimuli. Moreover, studies have shown that sometime MOF-encapsulated drugs, such as gentamicin [24], nalidixic acid [25], and vancomycin [26], have higher antimicrobial efficacy compared to the drug alone, which was attributed to the synergistic and additive effects of various mechanisms of antimicrobial action [23]. Despite the demonstrable antimicrobial efficacy of loaded MOFs, their granular nature makes it challenging for their use for purpose-specific applications, such as wound dressing or suture materials. Hence, several studies have also investigated various MOF composites including polymer composites of MOFs combined with biocompatible chitosan [25], poly (lactic-co-glycolic acid) (PLGA), and polycaprolactone (PCL) [26], for enhanced release in real-world applications.

Ciprofloxacin (CIP) is an antibiotic from the fluoroquinolone class that is notably effective against Gram-negative bacteria like *E. coli*, *H. influenza*, and used widely for treatment of serious infections, like pneumonia, primarily via oral administration. CIP can also be used in eye-drops, and in ointments for external applications. However, there are various concerns raised towards the topical use of ciprofloxacin [27], as topical formulations of antibiotics like creams, ointments, and other on-skin dosage contribute greatly to the fast emergence of AMR [28], limiting the further scope of application of CIP. Recently, CIP has been integrated into polymer composites, to explore their potential integration into wider antimicrobial applications [29,30]. However, this approach often suffers from the uncontrolled release of the drugs [31]. To address this issue, we explored possible integration of CIP into two isostructural Zr-based MOFs; UiO-66 and UiO-66-NH₂ combined with biodegradable PCL for more controlled and sustained delivery, as shown in Scheme 1 [32,33]. UiO MOFs have attracted much attention for applications in drug delivery, due to their relative stability, which makes them suitable for loading and release of various drugs, including hormones, antibiotics, and anticancer drugs. Several studies explore the



Scheme 1. An illustration of ciprofloxacin loaded MOFs and their integration into PCL composite for effective antibacterial activity.

synthesis and characterisation of UiO-66 MOFs as drug carriers, along with their in vivo and in vitro performance [34–37]. Nasrabadi et al. have explored the loading of ciprofloxacin into UiO-66 MOFs [38].

Despite the promising studies incorporating UiO MOFs, there are still challenges in using them as effective drug carriers for practical applications, especially due to their granular nature, which can lead to aggregation, sedimentation, and poor dispersion. This can in turn, affect the release kinetics, drug release profile, and limit their applications. One of the possible solutions is to integrate the granular MOFs into polymer membranes (Scheme 1). Hence, in this study loading of CIP into the MOFs was optimised and followed by integration into biodegradable PCL membranes. The antimicrobial activity of the resulting PCL composites of CIP-loaded UiO-66 and UiO-66-NH₂, was then tested against *S. aureus* and *E. coli* and compared to the antimicrobial efficiency of ciprofloxacin, PCL and the MOF alone.

2. Experimental

2.1. Synthesis

2.1.1. Materials

Zirconium (IV) tetrachloride (98%, anhydrous), terephthalic acid (98%), Phosphate Buffer Saline (PBS) tablets (P4417), and polycaprolactone with average molecular weight of 45,000, were purchased from Sigma Aldrich. 2-Aminoterephthalic acid (99%) was purchased from Thermo Scientific. Ciprofloxacin (>98%) was purchased from Tokyo Chemical Industry (TCI). All chemicals were used without any further purification. All solvents (HPLC grade) were obtained from Fisher Scientific.

2.1.2. Synthesis of pristine UiO-66

A mixture of ZrCl₄ (0.6316 g, 2.703 mmol) and terephthalic acid (0.8964 g, 5.408 mmol) along with dimethylformamide (DMF, 16 mL) and concentrated HCl (0.5 mL) were placed in a 40 mL Teflon lined glass vial which was then sonicated at 25 °C for 20 min. The mixture was then placed in an oven at 120 °C for 24 h with a heating rate of 10 °C per minute followed by cooling down to 25 °C at a rate of 2 °C per minute. The precipitate formed was then vacuum filtered using a Buchner funnel and washed twice with excess DMF. Activation of MOF was performed by immersing the pristine MOFs in fresh methanol three times for 24 h followed by drying in a vacuum oven at 115 °C for another 24 h. The obtained product was a white crystalline powder. FT-IR (cm⁻¹): 1661 (w), 1586 (m), 1506 (w), 1391 (s), 742 (s), 661 (s).

2.1.3. Synthesis of UiO-66-NH₂

In a 40 mL Teflon lined glass vial, a solution containing ZrCl₄ (0.125 g, 0.536 mmol), DMF (5 mL) and concentrated HCl (1 mL) was sonicated at 25 °C for 20 min. To the resulting mixture additional DMF (10 mL) and 2-aminoterephthalic acid (0.134 g, 0.740 mmol) were added and sonicated for a further 20 min. The resulting solution was placed in an oven at 80 °C for 24 h with a heating rate of 10 °C per minute and a cooling rate of 2 °C per minute to reach 25 °C. The obtained solid was vacuum filtered using a Buchner funnel and washed three times with DMF. Activation of MOF was performed by immersing the MOFs in fresh methanol three times for 24 h and then placing in a vacuum oven at 115 °C for another 24 h. The resultant product was a pale-yellow crystalline powder. The FT-IR (cm⁻¹): 3353 (b), 1653 (m), 1568 (m), 1432 (m), 1384 (s), 1257 (m), 764 (m), 658 (s).

2.1.4. Ciprofloxacin loading in Zr-MOFs

Activated pristine UiO-66 (0.1 g) and UiO-66-NH₂ (0.1 g) were placed in separate 16 mL Teflon lined glass vials containing a solution of ciprofloxacin (CIP, 0.2 g) that was dissolved in 10 mL of methanol. The mixtures were sealed and stirred at 300 rpm at room temperature for 5 days. The resulting mixtures were centrifuged for 20 min and then carefully washed three times with methanol (10 mL) and vacuum dried in an oven at 60 °C overnight to obtain the CIP-loaded MOFs. CIP-loaded UiO-66 (UiO-66-CIP) appeared as a white powder, and UiO-66-NH₂-CIP as a pale-yellow powder. FT-IR (cm⁻¹): UiO-66-CIP: 1613 (m), 1586 (m), 1499 (m), 1472 (w), 1393 (m), 1374 (m), 1285 (m); UiO-66-NH₂-CIP: 1613 (m), 1586 (m), 1498 (m), 1472 (w), 1373 (m), 1285 (m).

2.1.5. Preparation of polycaprolactone-MOF hybrid drug carriers via solvent-casting

Polycaprolactone (PCL) pellets (0.2 g) were placed in a beaker containing chloroform (15 mL) and stirred using a magnetic stirrer for 30 min, until all pellets were dissolved. Separately, samples of UiO-66-CIP, UiO-66-NH₂-CIP and CIP (5 mg) were weighed and ground using a mortar and pestle. Subsequently, 5 mL of the PCL solution was placed in 10 mL glass vials and the ground samples were added under stirring for a further 20 min. The mixtures were then left to set overnight and the chloroform to evaporate to form the composite membranes.

2.2. Material characterisation

Powder X-Ray Diffraction (PXRD) was recorded at ambient temperature using a Bruker D8 diffractometer with Cu K (λ = 1.54018 nm, 1600 W) source. Fourier transform infrared (FT-IR) analysis was carried out using a PerkinElmer Spectrum 100 ATR FT-IR Spectrometer in the range 650–3500 cm⁻¹. Thermogravimetric analysis (TGA) was carried out using a Q5000IR thermogravimetric analyser (TA); the sample was placed in a platinum pan and heated under nitrogen at a rate of 5 °C per minute to reach a final temperature of 600 °C, and the data were processed with the TA instruments Universal Analysis software. Scanning electron microscope (SEM) images of the pristine and loaded MOFs and of the composite samples were obtained using a FEI Quanta 400 E-SEM instrument under vacuum conditions. Samples with PCL were sputter-coated with gold prior to SEM analysis. UV-Vis analysis was performed using on a Jenway spectrophotometer - 7205 model.

Information on the specific surface area and internal pore structure was obtained from N₂ adsorption at 77 K on a Micromeritics 3Flex volumetric gas sorption analyser. Each material (~10–25 mg) was degassed prior to the experiment (388 K, ~8 h, 1 × 10⁻⁶ mbar). Helium was used for free-space determination following isothermal data collection. Nitrogen and helium were supplied by Air Liquide with purity >99.999%. Pore volume distribution as a function of pore width was calculated from the N₂ adsorption data using a density functional theory (DFT) fitting and a cylindrical pore – NLDFIT Tarazona Esf = 30 K model. The BET surface area was determined following the procedure outlined in ISO 92773. A Rouquerol correction was applied to the BET fitting to

calculate surface areas. A resultant correlation function of >0.9999 was observed for each material and a positive intercept (Fig. S1).

2.3. Drug release studies

Release of CIP in sink conditions was studied in phosphate buffered saline (PBS) at pH 7.4, acidified PBS with hydrochloric acid at pH 3 and pH 6, sodium hydrogen carbonate at pH 8.5 and accelerated aging solution (AA). AA was prepared by adding 1 mL of Tween-80, 50 mL of methanol and 50 mL of acetonitrile in PBS (500 mL) and the resulting mixture was stirred for 10 min. All release studies were repeated three times to check reproducibility. Quantitative determination of the CIP in release studies was carried out using UV-Vis spectroscopy. A calibration plot (Figures S2.1 and S2.2, and Figures S3.1, S3.2 and S3.3 in SI) was obtained by the following procedure: CIP (0.1 mg) was completely dissolved in PBS and AA (10 mL), to make stock solutions. From the stock solutions various concentrations were prepared ranging between 1.33 and 0.01 μg mL⁻¹. The λ_{max} was identified at 270 nm for samples in PBS and 271 nm for those in AA (Figure S2.3 and S2.4 in SI). The absorbance of each dilution was measured using the λ_{max} to plot the calibration curve.

Powdered samples of UiO-66-CIP and UiO-66-NH₂-CIP (4 mg) and the polymer samples; PCL-UiO-66-CIP and PCL-UiO-66-NH₂-CIP (9 mg), were placed in 16 mL glass vials. Release media (10 mL) was pre-conditioned at 37 °C and then added to each vial containing the relevant samples and sealed. The vials were placed in a water-bath to maintain a constant temperature of 37 °C.

For the release studies, 1 mL of the supernatant was extracted and immediately replaced with fresh media to ensure sink conditions, at specific time points ranging between 1 and 168 h. The concentration of CIP was determined using UV-Vis spectrophotometry. The concentration of CIP released at each time point was calculated using this equation:

$$C_{t_{\text{corr}}} = C_t + \frac{v \sum_{c=0}^{t-1} C_t}{V} \quad (1)$$

Equation (1) was used for calculating the corrected concentration, where C_{t_{corr}} is the corrected concentration at time, C_t is the calculated concentration of CIP using the calibration at time, v is the volume of the extracted sample and V is the total volume of the release solution.

2.4. Antimicrobial analysis

The antimicrobial activities of 1 mg of the pristine MOFs, the CIP loaded MOFs and the PCL-MOF-CIP composites were assessed against Gram-positive and Gram-negative bacterial strains *S. aureus* NCTC 6571 and *E. coli* NCTC 12923, using the zone of inhibition assay. In addition, samples without MOFs such as CIP, PCL and PCL-CIP were also tested for comparison. The bacterial culture was prepared overnight on Tryptic Soya Agar (TSA). Two-three colonies were then diluted in distilled and sterile water and the turbidity was adjusted to 5 × 10⁸ Colony Forming Units (CFUs) mL⁻¹, according to the McFarland standard [39]. The bacterial suspensions were then spread on Mueller-Hinton agar and subsequently the weighed samples of MOFs and their composites were carefully placed on the plate. The plates were then incubated for 24 h at 37 °C, before being imaged. The antimicrobial activity was determined by measuring the diameter of the inhibition zones. In addition, further antimicrobial tests were performed on the PCL-MOF hybrid materials after having been in the PBS release study for 7 days. The PCL composites were removed from the PBS release solution and washed with excess PBS. They were then placed on agar plates that contained the bacterial strains and incubated for 24 h at 37 °C. Additionally, 100 μL of the PBS release solution was extracted and spread on the agars containing the bacteria and similarly incubated for 24 h at 37 °C.

3. Results and discussion

UiO-66 and UiO-66-NH₂ were synthesized using previously reported method, with minor modifications [40]. Pristine and CIP-loaded UiO-66 and UiO-66-NH₂, and their PCL composites, were characterised using various techniques, followed by drug release and antimicrobial assay, as detailed below.

3.1. Characterisation of materials

3.1.1. Powder x-ray diffraction analysis

Powder x-ray diffraction (PXRD) patterns of pristine MOFs and their polymer composites are shown in Fig. 1. The position of characteristic Bragg diffraction peaks for both UiO-66 and UiO-66-NH₂ MOFs agree with literature as well as calculated patterns, indicating successful synthesis [41]. The same diffraction patterns can also be observed in CIP loaded MOFs, with two sharp peaks at $2\theta = 7.41^\circ$ and 8.53° , indicating the stability and preservation of its crystallinity upon post-synthetic loading of CIP. For PCL composites, the characteristic peaks for the MOFs can be faintly observed, indicating the presence of the MOFs inside the composite in relatively small proportion. In addition, peaks pertaining to the PCL structure can be well observed at $2\theta = 21.4^\circ$, 22.0° and 23.7° that are associated with the (100), (111), and (200) planes of

the orthorhombic crystal lattice of PCL [42]. PXRD data indicate that the MOF is stable and retains its crystallinity upon post-synthetic loading of CIP.

3.1.2. Fourier-transform infrared spectroscopy

Fourier-transform infrared spectroscopy (FT-IR) spectra of UiO-66, UiO-66-NH₂ and their PCL composites are shown in Fig. 2. The spectra shown agree with literature [43,44]. Characteristic bands observed at 1661 cm^{-1} and 1586 cm^{-1} correspond to asymmetric stretches of the O=C=O groups for Pristine UiO-66. While strong band at 1391 cm^{-1} is for the symmetric stretch from the carboxylate group of the BDC linker, peaks observed at 1506 cm^{-1} are a result C=C vibrations from the aromatic rings. Characteristic bands pertaining to the O-H bending of the organic linker and the Zr-O stretching of the metal-ion cluster can be observed at 742 cm^{-1} and 661 cm^{-1} , respectively. A weak absorption band at 3353 cm^{-1} for pristine UiO-66-NH₂ corresponds to the symmetric and asymmetric vibrations of NH₂ from the NH₂-BDC linker. Peaks found at 1568 cm^{-1} and 1432 cm^{-1} can be traced to the asymmetrical stretches of the carboxylate group and reaction with Zr⁴⁺. Bond stretching between the nitrogen of the amine group and the carbon of the aryl group were identified by the peaks at 1384 cm^{-1} and 1257 cm^{-1} . The IR results also display clear evidence of CIP drug loading in both UiO-66-CIP and UiO-66-NH₂-CIP with distinguishable bands at

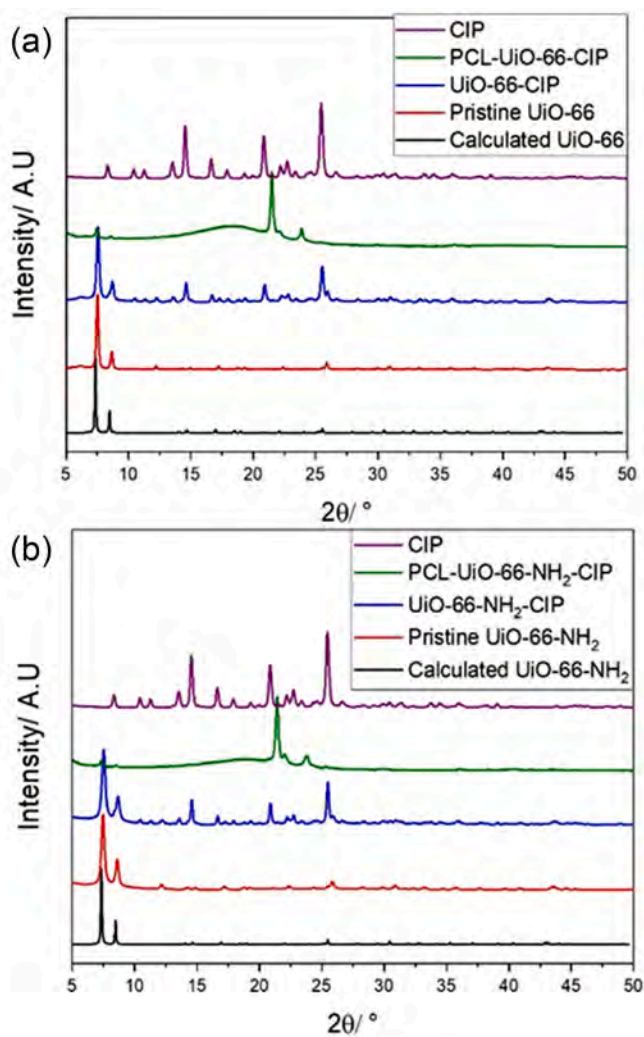


Fig. 1. (a) PXRD patterns of pristine UiO-66, UiO-66-CIP, PCL-UiO-66-CIP and CIP; (b) PXRD of pristine UiO-66-NH₂, UiO-66-NH₂-CIP, PCL-UiO-66-NH₂-CIP and CIP (b).

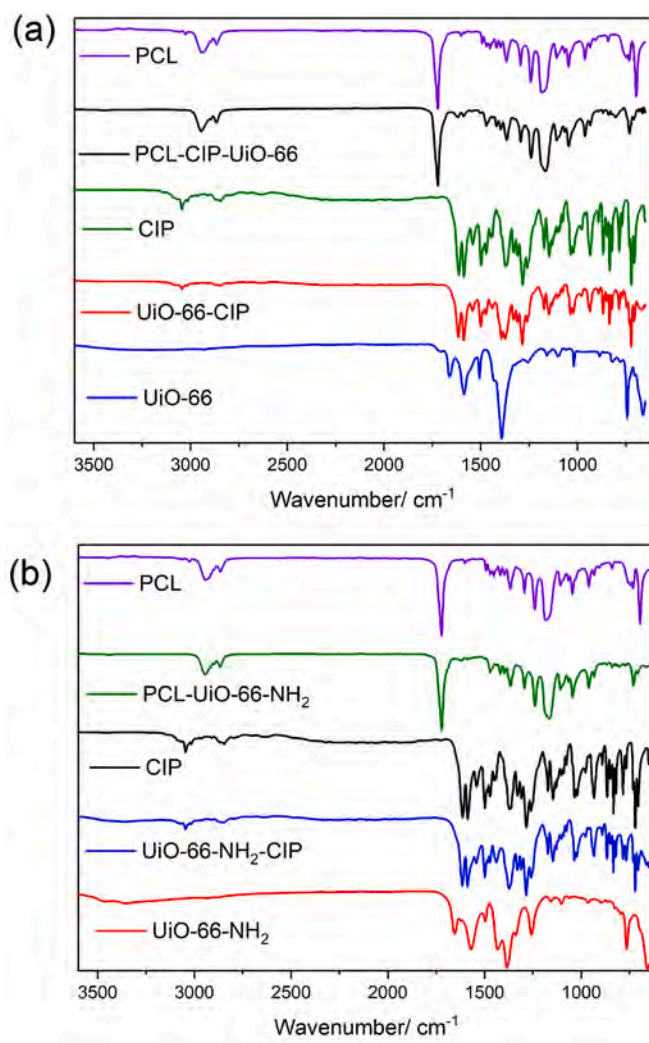


Fig. 2. (a) IR spectra of pristine UiO-66, UiO-66-CIP, PCL-UiO-66-CIP and CIP; (b) IR spectra for pristine UiO-66-NH₂, UiO-66-NH₂-CIP, PCL-UiO-66-NH₂-CIP and CIP.

2846, 1613 and 1472 cm^{-1} which can be traced back to peaks found for CIP (Fig. 2). The band at 2846 cm^{-1} is indicative of a nitrogen-carbon bond stretch, the peak at 1613 cm^{-1} is attributed to the C=O carbonyl stretch of quinoline, and the band at 1472 cm^{-1} corresponds to carbon-nitrogen stretching in CIP. The infrared spectrum of the PCL-UiO-66-CIP and PCL-UiO-66-NH₂-CIP were compared with the pristine MOFs and their PCL composites (Fig. 2). The presence of CIP in the loaded MOFs is identifiable from the presence of a weak band at 1470 cm^{-1} which is in coherence with the bands present in the IR spectra of CIP [45]. The high similarities between the spectra for PCL-UiO-66-CIP and PCL-UiO-66-NH₂-CIP is obvious due to the high proportion of PCL in the composites. The bands found at 2944 cm^{-1} and 2866 cm^{-1} represent asymmetrical and symmetrical CH₂ stretching in PCL, respectively. The band found at 1721 cm^{-1} is indicative of C=O carbonyl stretching and the peak at 1293 cm^{-1} represents C-O and C-C stretching. The bands at 1239 cm^{-1} and 1165 cm^{-1} are attributed to asymmetrical and symmetrical stretching of O-C-O bonds, respectively.

3.1.3. Thermal gravimetric analysis

TGA of the pristine UiO-66 and UiO-66-NH₂ (Fig. 3), indicate that they both show weight loss in three stages. The first stage, between 30 °C and 100 °C, accounts for weight loss of 17.1% for UiO-66 and 17.9% for UiO-66-NH₂ and occurs due to the loss of residual solvents and water. The next stage can be associated with the dehydroxylation of the Zr-oxo clusters, between 100 °C and 400 °C, and accounts for a loss of 13.5% for UiO-66 and 20.7% for UiO-66-NH₂, respectively. In addition, a sharp weight loss around 350 °C can be attributed to the decomposition of ciprofloxacin inside the pores [46]. The final stage of weight loss occurs at around 500 °C for UiO-66 and 525 °C for UiO-66-NH₂ due to complete thermal degradation of the MOFs, including organic ligands (terephthalic acid or 2-aminoterephthalic acid) and zirconium clusters.

Thermogravimetric analysis of PCL-UiO-66-CIP and PCL-UiO-66-NH₂ (Fig. 4) primarily show close resemblance to PCL due to its high proportion in the composition [47]. Two stages of weight loss are observed, with the first stage accounting for the decomposition of PCL at 225 °C resulting into 95.3% loss in mass [47]. The second stage is extremely small, but clearly identifiable at 500 °C reflects the degradation of UiO-66 and agrees with the decomposition temperature of the MOF as seen in Fig. 4. This results in a mass loss of 2.8%. It was also found that 50% of mass was lost at 395 °C in pure PCL and at 373 °C in PCL-UiO-66-CIP.

3.1.4. Scanning electron microscopy imaging and energy dispersive spectroscopy

The morphology of the pristine Zr-MOFs was examined using SEM, which confirmed the homogeneity of the samples (Fig. 5). From the SEM images, it is observed that the CIP loaded MOFs have similar

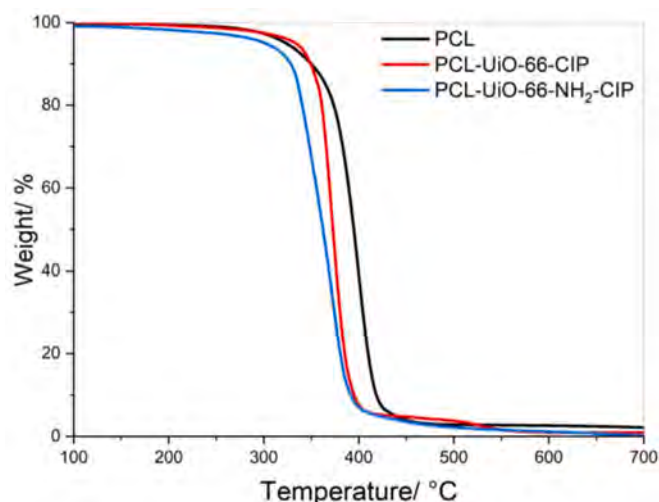


Fig. 4. TGA for PCL composites of PCL-UiO-66-CIP and PCL-UiO-66-NH₂-CIP.

morphologies to that of the pristine MOFs.

The PCL composite morphology was influenced by the amount of loaded MOF incorporated into the polymer matrix and this agrees with previously published research [44]. The SEM images of the PCL composites (Fig. 6) show a difference in surface morphology between the composite, PCL-CIP and the PCL alone. Pure PCL has a relatively smooth surface, in contrast to PCL-UiO-66-CIP and PCL-UiO-66-NH₂-CIP, where the embedded particles can be observed and contribute to a rougher surface in the case of the composites.

Energy dispersive spectroscopy (EDS) of the MOF-Polymer composites is shown in Fig. S4 of SI. From the analysis, it can be observed that the polymer composites are mostly comprised of C and O (about 98%), as expected from PCL, the organic linkers, and ciprofloxacin. In addition, peaks observed for the presence of Zr and F corresponds to the presence of MOFs, and ciprofloxacin, respectively, throughout the composites.

3.1.5. Surface area and pore size analysis

As classified by IUPAC [48], both ciprofloxacin doped MOFs exhibited Type I nitrogen sorption isotherms indicating microporous materials (Fig. 7), with uptake governed by micropore volume, similar to the native pristine MOF samples. In comparison to the respective pristine MOFs, both ciprofloxacin doped MOFs exhibit a

Reduced total quantity of adsorbed N₂, indicating a loss in porosity for the samples. This is also reflected in the diminished surface areas and total pore volumes observed for the samples. To determine surface area, BET plots were taken for each sample (Fig. S1) and fitted using the

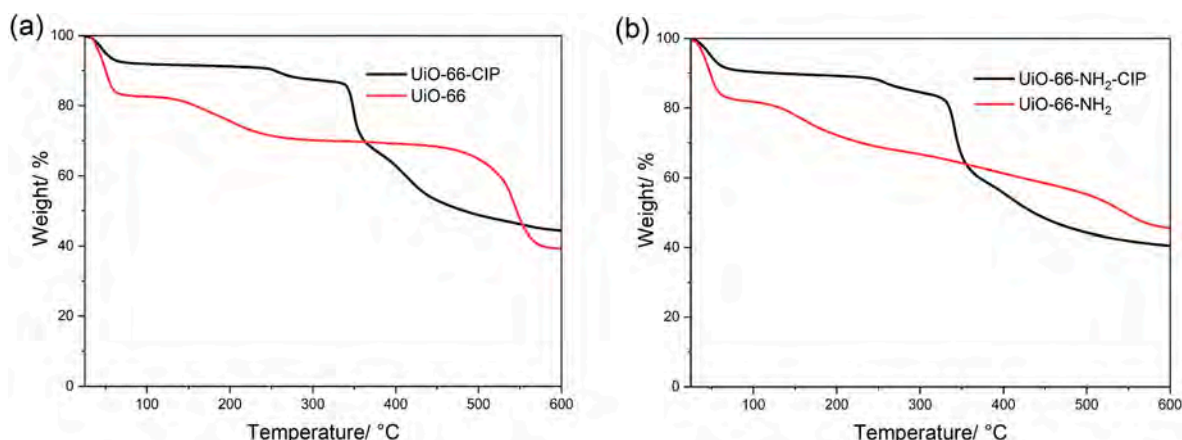


Fig. 3. TGA for (a) UiO-66 and uiO-66-cip. And for (b) uiO-66-nh₂-cip and uiO-66-nh₂-cip

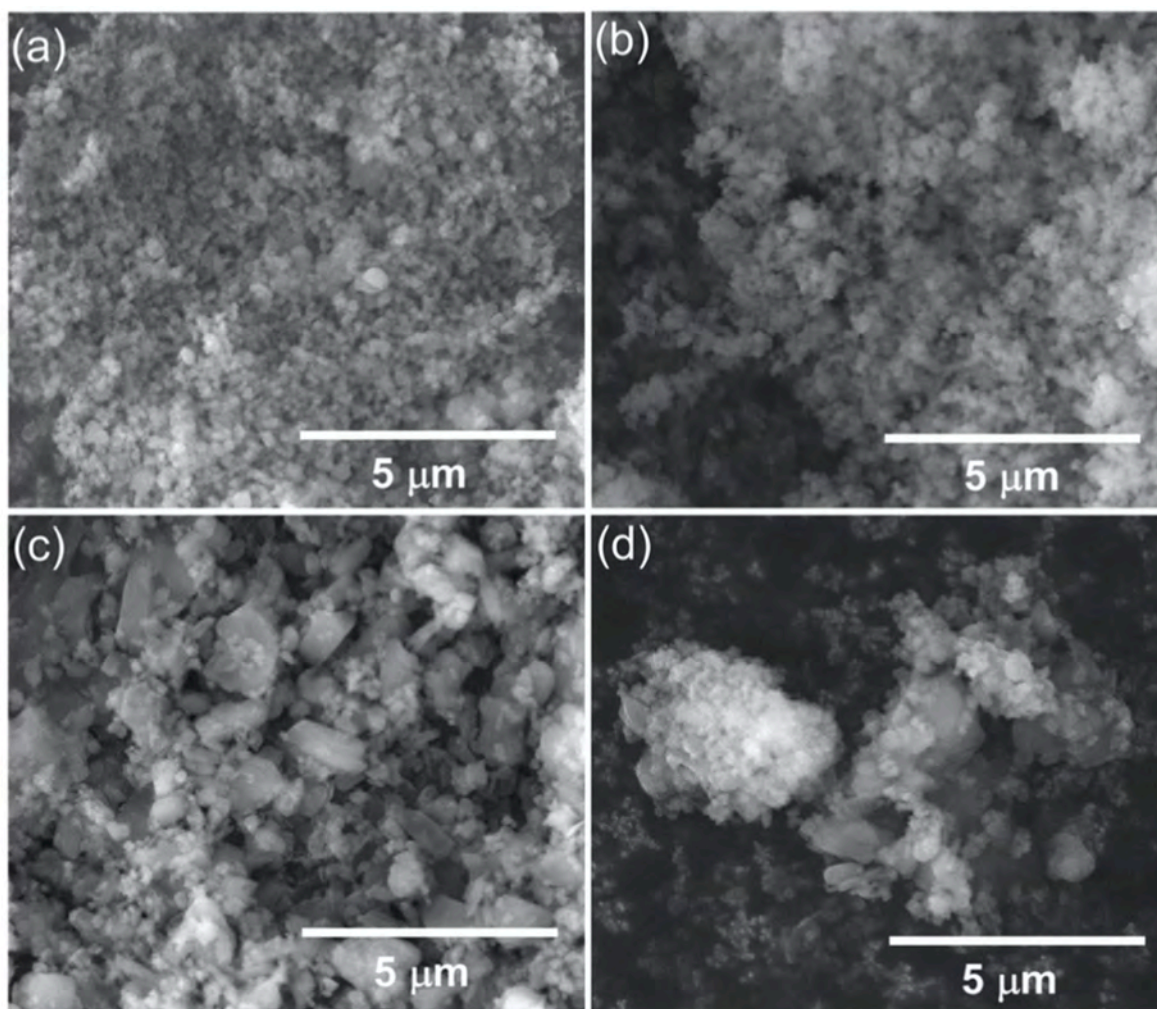


Fig. 5. SEM images of Zr-MOFs and loaded Zr-MOFs. (a) Pristine UiO-66, (b) Pristine UiO-66-NH₂, (c) UiO-66-CIP, (d) UiO-66-NH₂-CIP.

Rouquerol method [49], ensuring a positive y-intercept and the highest correlation function (R^2) values. Table 1 summarises the calculated pore characteristics of the MOF samples compared to the pristine UiO-66 and UiO-66-NH₂ previously measured [50].

Comparing the surface area and total pore volume of the CIP doped MOFs to the pristine samples, it can be observed that UiO-66-CIP undergoes ~70% loss in surface area and 76% loss in total pore volume in comparison to pristine UiO-66, where the UiO-66-NH₂-CIP, experiences ~30% loss in surface area and 27% loss in total pore volume in comparison to pristine UiO-66-NH₂. This reduction could be due to either degradation of the original pore network or guest molecules occupying available pore volume. From PXRD data, we can infer that no significant degradation to the primary structure of the MOFs occurred upon introduction of CIP.

Changes to the available pore volume in the samples were attained by analysis of the calculated pore size distributions and the cumulative pore volumes. Pore size distributions and cumulative pore volume of samples were calculated by fitting the isotherms to DFT models, with the Tarazona cylindrical pore NLDFT model achieving the best goodness of fit. The results were compared to the pristine UiO-66 and UiO-66-NH₂, previously measured [50] (Fig. 8), with the calculated losses to available pore volume for each of the known pore sizes of the pristine MOFs presented in Table 2.

Based on the pore size distributions presented in Fig. 8, introduction of ciprofloxacin causes no change to the size of the pores of the two MOFs, indicating that pore sizes remain the same as the pristine MOFs

and suggesting no degradation of the pore network/structure occurs in the samples. However, a reduction in available pore volume is observed for both samples and observable in both the differential pore volume distribution and cumulative pore volume displayed in Fig. 8. When compared to the pristine MOF, virtually no mesoporosity (pores between 20 and 50 Å in size) is observed for UiO-66-CIP with some reduction in microporosity, suggesting the mesopores of UiO-66 were completely filled with ciprofloxacin and some micropores are filled or access is blocked. Considering ciprofloxacin is a large molecule with a max length of ~12 Å and max width ~8 Å, occupying larger sized pores would explain the major reduction in available volume for pores ≥ 8 Å. A reduction in available pore volume for pores < 8 Å is also observed and could be due to blocked access in the known pore network. For UiO-66-NH₂-CIP, a much smaller reduction in cumulative pore volume was observed in comparison to the UiO-66-CIP MOF. This is in part to the low level of intrinsic mesoporosity in the pristine UiO-66-NH₂ sample in the first place. The greatest loss in available pore volume in UiO-66-NH₂-CIP is observed for the 16.7 Å pore size, representing a 54% decrease in accessible pore volume. In comparison, the two smaller pores, 5.9 and 10.2 Å only observe a 21% and 35% reduction, indicating that the majority of the ciprofloxacin must sit in the 16.7 Å pores.

3.2. Drug release studies

Release of CIP was monitored over seven days (Fig. 9), in either PBS at pH of 7.4, or accelerated ageing media and at a constant temperature

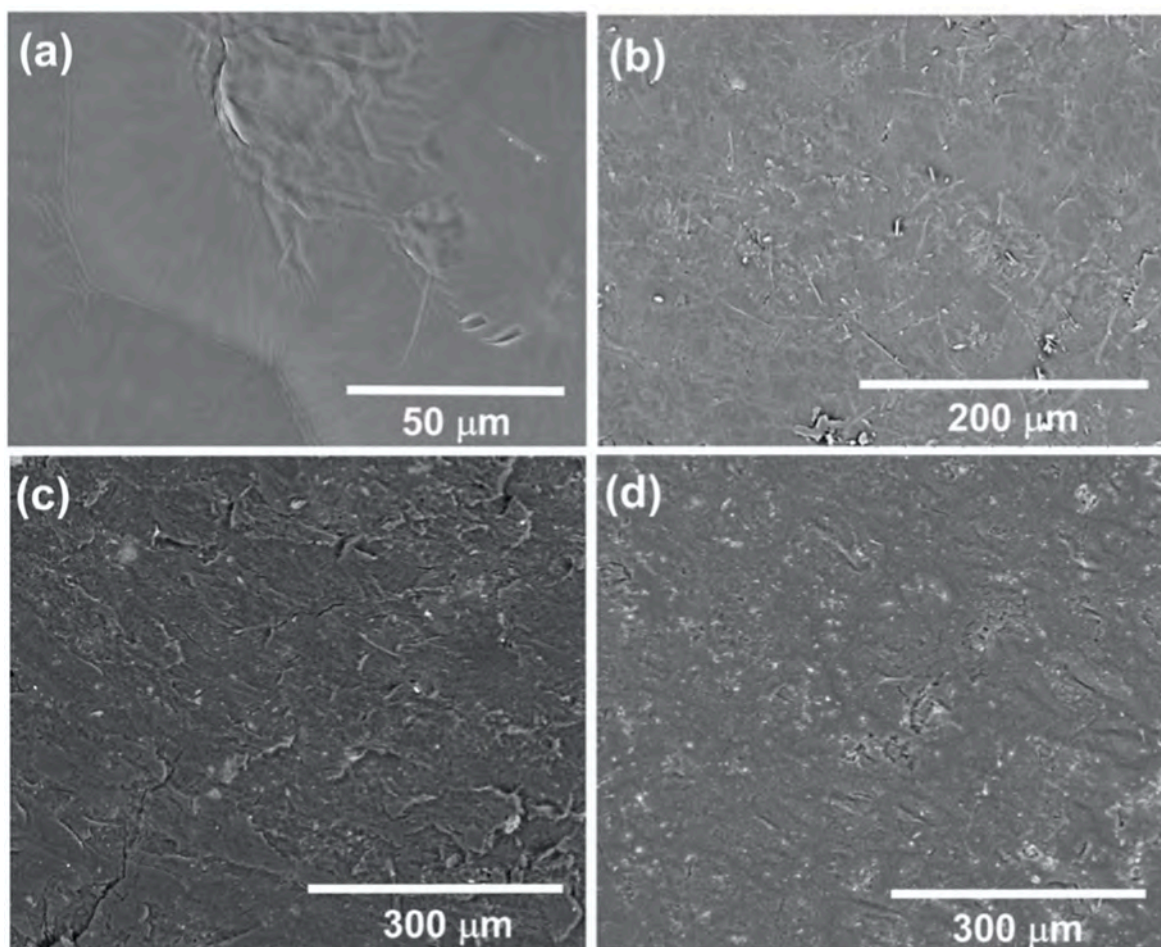


Fig. 6. SEM images of the polymer composites. (a) PCL, (b) PCL-CIP, (c) PCL-UiO-66-CIP, (d) PCL-UiO-66-NH₂-CIP.

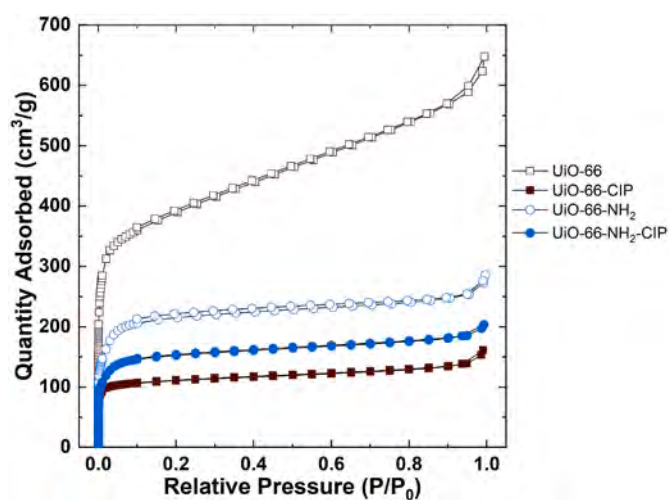


Fig. 7. Nitrogen adsorption-desorption isothermal cycles of pristine MOFs and ciprofloxacin loaded MOFs.

of 37 °C, to mimic body temperature. The results (average values of three repeats) clearly indicate that the MOF-CIP samples always released a greater quantity of CIP in both solutions, when compared to the polymer-MOF composites. In PBS, UiO-66-NH₂-CIP showed the highest concentration after 7 days at 34.1 μg mL⁻¹ release and of about 8.5% by weight, which was significantly higher than that of UiO-66-CIP, with a

Table 1

Pore characteristics of pristine and CIP-loaded UiO-66 and UiO-66-NH₂ from N₂ sorption analysis at 77 K.

Sample	BET Surface Area (m ² g ⁻¹)	Total Pore Volume ^a (cm ³ g ⁻¹)
UiO-66 [50]	1455.7 ± 2.2	0.913
UiO-66-CIP	433.7 ± 0.3	0.216
UiO-66-NH ₂ [50]	865.2 ± 5.9	0.394
UiO-66-NH ₂ -CIP	610.8 ± 2.4	0.288

^a Single point adsorption volume taken at P/P₀ 0.94.

concentration of 24.5 μg mL⁻¹, corresponding to 6.1%. However, the difference in drug release was not as significant in AA solution with only about 1.32 μg mL⁻¹ variation in concentration, due to the faster polymer degradation in that media. The higher concentration of CIP released by UiO-66-NH₂ can be due to the protonation of the amine group at that pH [51]. A common trend that can be seen in the CIP release in AA is that UiO-66-CIP always presents a higher released concentration. While this seemed to be the case in PBS, UiO66-CIP was quickly outperformed by UiO-66-NH₂-CIP after the 24-h time point. This may be due to the relatively slow release of CIP resulting from supramolecular interactions between carboxylate group of CIP and NH₂ groups of UiO-66-NH₂. Due to lack of such interactions in UiO-66-CIP, a higher release is likely at the early stages. The release behaviour found in AA is more in line with previous finding that reported UiO-66 and UiO-66-NH₂ displaying similar drug release after 72 h [38]. The data indicate that AA promotes greater release for the MOF-CIP samples, especially for UiO-66-CIP which released 39.5 μg mL⁻¹. This concentration dropped to 24.5 μg

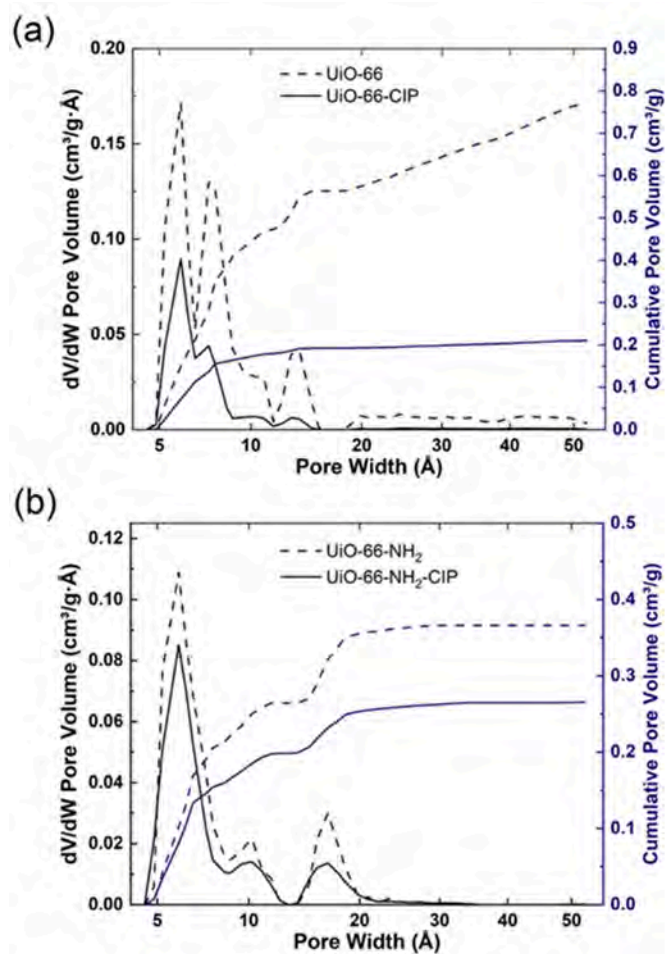


Fig. 8. Pore size distribution and cumulative pore volume of (a) UiO-66 samples, and (b) UiO-66-NH₂. Fitted with a Tarazona cylindrical pore NLDFT model.

Table 2

Percentage loss in available pore volume compared to pristine MOF pores (UiO-66/UiO-66-NH₂) from N₂ sorption analysis at 77 K.

	Percentage loss/%			
Sample	5.9/5.9 Å	7.7/10.2 Å	13.8/16.7 Å	20-50 Å range
CUiO-66-CIP	-47%	-66%	-86%	-91%
CUiO-66-NH ₂ -CIP	-21%	-35%	-54%	-6%

mL⁻¹ in PBS. This could be attributed to the presence of methanol in the AA suspension that caused the rapid release of CIP from the MOF and the polymer degradation.

The polymer composite samples; PCL-UiO-66-CIP, PCL-UiO-66-NH₂-CIP and PCL-CIP released similar concentrations of CIP in both PBS and AA. The release of CIP is much smaller with the addition of PCL than without it. The concentration of drug released by the three composite samples after 168 h is similar in all three cases. In both PBS and AA solutions, PCL-CIP has the highest drug release at all times, compared to the other composites. For the MOF PCL composites, similar trend was observed for the UiO-66-CIP and PCL-UiO-66-CIP, with a higher drug release of 1.69 µg mL⁻¹ in PBS for the latter initially, but it is overtaken by the PCL-UiO-66-NH₂-CIP (2.45 µg mL⁻¹) at the 24-h time point. However, unlike UiO-66-CIP, the concentration released by PCL-UiO-66-CIP (4.57 µg mL⁻¹) quickly reached higher than PCL-UiO-66-NH₂-CIP (4.10 µg mL⁻¹) after 48-h. The release performance of PCL-UiO-66-CIP and PCL-UiO-66-NH₂-CIP is much more straightforward in AA

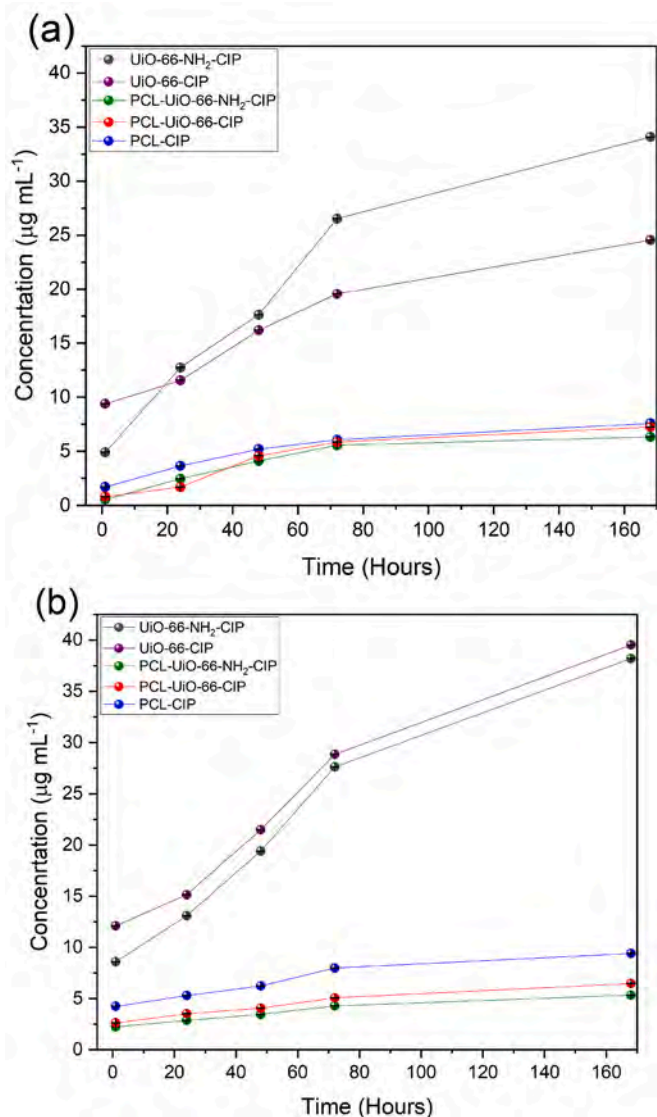


Fig. 9. Drug release profile in (a) PBS (b) and AA for UiO-66-CIP, UiO-66-NH₂-CIP, and their PCL composites.

solution and shows that PCL-UiO-66-CIP always releases a greater concentration of CIP, due to faster polymer degradation. Therefore, PCL-UiO-66-NH₂-CIP demonstrates an overall slower and more controlled drug release than PCL-UiO-66-CIP even though it is not by a large margin. Overall, the main reason for the smaller release in the case of the PCL samples compared to the MOF samples is the slowed down release of the CIP, not only by its rate of diffusion through the MOF pore system but due to the polymer too. The CIP concentration released from the polymer composites is well within the Minimum Inhibitory Concentration (MIC) against both Gram-positive and Gram-negative bacteria, such as *E. coli* and *S. aureus*, that is in the range of 0.21–3.42 µg mL⁻¹ [52], and is well maintained within the MIC throughout the 7 days of testing [53].

Therapeutic concentrations of ciprofloxacin ranges depending on age, demographic, bioavailability, and dosage form. Effective intravitreal injection concentrations above 1 µg mL⁻¹ were shown to be effective in inhibiting up to 90% of microorganisms linked to endophthalmitis [54]. And in other studies, ciprofloxacin was effective in treating respiratory tract infections at maximum bronchial secretion concentration of 2.5 µg mL⁻¹ [55]. The concentrations observed here from release studies lie within the range of effective concentrations needed to treat various site-specific infections, which makes such

composite system ideal for the development of biodegradable implants for treatment of infection sites.

The effect of pH on drug release behaviours from the polymer composites was studied in acidic, basic, and near neutral conditions for 72 h pH plays a significant role on the amount of drug released. As shown in Fig. 10, for pH of 3 and 8.5, both composites showed burst release of ciprofloxacin, with highest concentration peaking at 24 h. At pH of 6, slow and controlled release of ciprofloxacin was observed, similarly to pH 7.4 (Fig. 7). This could be explained by pH-dependent factors that govern MOF-drug interactions, including the stability of MOFs at various pH, surface charge, pK_a values, and chemistry of the functional groups. Ciprofloxacin is a zwitterion with two functional groups of $-\text{COOH}$ and $-\text{NH}$ with pK_a of 6.18 and 8.76, respectively. The isoelectric point governs the surface charge at various pH, and for UiO-66 and UiO-66-NH₂ it is 5.6 [56]. At lower pH, the burst effect can be a result of the accumulation of positive charge on the MOF surface via the breaking of coordination bonds between Zr-metal sites and protonated $-\text{OH}$ groups, in addition to the protonation of the amine groups of UiO-66-NH₂ leading to the electrostatic repulsion of positively charged ciprofloxacin from the surface and expulsion from MOF pores. Likewise, at higher pH, the anionic nature of ciprofloxacin and the accumulated negative charge on MOFs can also contribute to weaker binding, and enhanced release. In addition, relatively lower stability of the PCL and the MOFs at pH 3 and 8.5 will also result in faster degradation of the polymer and partial collapse of the MOFs, hence aiding further to release of CIP from the composite.

3.3. Antimicrobial analysis

The antimicrobial properties of all components were assessed by the disk diffusion method against Gram-positive and Gram-negative bacterial strains; *S. aureus* and *E. coli*, respectively, and the results are presented in Table 3. It was crucial to investigate the antimicrobial abilities of the pristine MOFs, pure CIP and PCL to compare their efficiencies against the loaded MOFs and their composites. In accordance with the literature, UiO-66 and UiO-66-NH₂ showed no antimicrobial activity against either bacterial strain [53]. The CIP was more effective against *E. coli* with a 66.2 mm zone of inhibition compared to *S. aureus* (49.4 mm). This supports previous research which states that CIP is more effective against Gram-negative bacterial strains such as *E. coli*, as it has a MIC value of 0.6 $\mu\text{g mL}^{-1}$ in comparison to *S. aureus* which has an MIC value of 0.7 $\mu\text{g mL}^{-1}$ [52]. This shows that it is easier for CIP to kill and inhibit *E. coli* growth compared to *S. aureus*, providing a larger zone of inhibition for the Gram-negative strain.

The incorporation of CIP into the MOFs; UiO-66-CIP and UiO-66-

NH₂-CIP and the further addition of the loaded MOFs into PCL significantly reduced the zones of inhibition compared to the CIP only, and the PCL-CIP, showing that CIP was released at a lower concentration within the 24-h assay when in the PCL-MOF composites. This is expected, as encapsulation of CIP inside the pores of the MOFs is likely to slow down the release of the drug compared to PCL-CIP composite where such encapsulation is absent. Pure PCL demonstrated antimicrobial ability of a 16.6 mm zone of inhibition in *E. coli* and showed no activity against *S. aureus* (Table 3). This agrees with the literature that states pure PCL has a higher bacterial inhibition efficiency against *E. coli* than *S. aureus*, and together with the higher efficacy of CIP against *E. coli*, it was expected that the PCL composites would be more effective against this bacterial strain than *S. aureus* [57]. This assumption was proven when PCL-UiO-66-CIP showed zones of inhibition of 38.3 mm and 28.3 mm for *E. coli* and *S. aureus*, respectively. The difference between the inhibition zones found for PCL-UiO66-NH₂-CIP was much smaller with 37.1 mm for *E. coli* and 35.4 mm for *S. aureus*. During the evaluation of the most effective PCL-MOF carrier, PCL-UiO-66-CIP outperformed PCL-UiO-66-NH₂-CIP against *E. coli* but was surpassed for *S. aureus*. Finally, it should be noted that PCL-CIP showed higher antimicrobial activity than PCL-UiO-66-NH₂-CIP and PCL-UiO-66-CIP in *E. coli*.

Table 4 shows the antimicrobial activity of the PCL composites after 7-days of immersion in PBS for the drug release study. It was observed that after 168 h in the release media the PCL-MOF-CIP composites still displayed antimicrobial activity that was similar to that observed before immersion, showing that the remaining antibiotic in the composite samples, a week post-immersion, was still releasing in the zone of inhibition assay at a concentration sufficient to cause similar, if not greater, zones of inhibition to the non-immersed samples (Table 3). These immersed composites showed greater inhibition for *E. coli* than *S. aureus* and this tendency had not changed from results found prior to the 7-day immersion (Table 3). PCL-UiO-66-CIP displayed a larger zone of inhibition than PCL-UiO-66-NH₂-CIP and PCL-CIP against both bacterial strains (Fig. S5 in SI). This resembles the behaviour of PCL-UiO-66-CIP against *E. coli* before the 7-day immersion as it also showed a higher inhibition than PCL-UiO-66-NH₂-CIP. These results show that the polymer composites are still releasing a significant amount of drug as the zones of inhibition are similar and, in some cases, larger than those observed in Table 3 potentially due to a faster release from a more degraded polymer, after seven days of immersion in PBS, pH 7.4. It was also observed that the PCL-MOF hybrid materials displayed a larger zone of inhibition against *E. coli* after the 7-day immersion period than before, again due to polymer degradation [58], hence, it enables the drug to diffuse through the polymer matrix into the agar plate more readily. However, in the case of *S. aureus*, there was a decrease in the inhibition

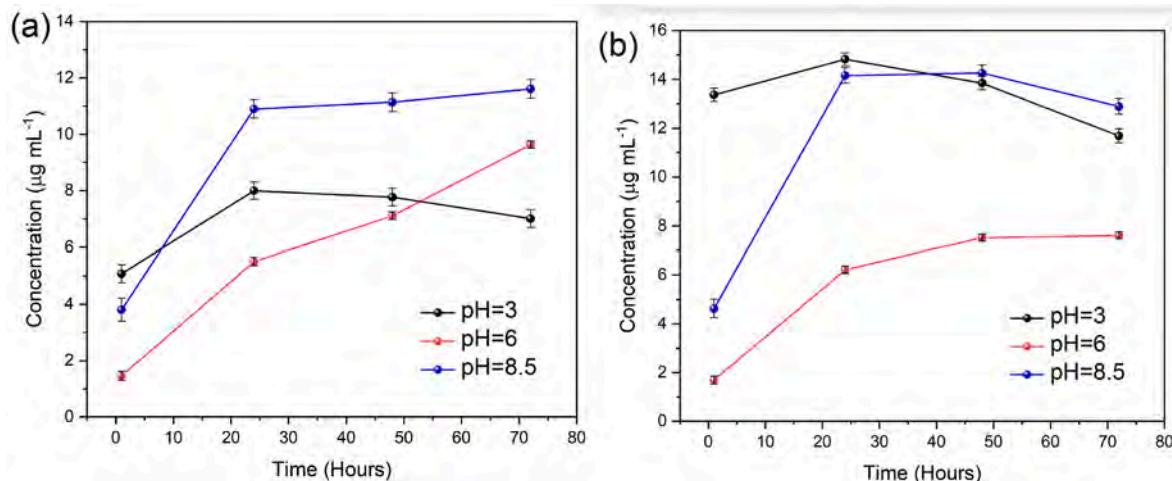


Fig. 10. Drug release profile at pH 3, 6 and 8.5 for (a) PCL-UiO-66-CIP and (b) PCL-UiO-66-NH₂-CIP are shown.

Table 3

The antimicrobial activity of CIP, PCL, Pristine Zr-MOFs and PCL composites against bacterial strains.

Bacteria	Zone of inhibition (mm)								
	CIP	PCL	PCL-CIP	Pristine UiO-66	Pristine UiO-66-NH ₂	UiO-66-CIP	UiO-66-NH ₂ -CIP	PCL-UiO-66-CIP	PCL-UiO-66-NH ₂ -CIP
<i>E. coli</i>	66.2 ± 3.1	16.6 ± 1.4	42.6 ± 2.2	0 ± 0	0 ± 0	43.2 ± 1.4	50.6 ± 2.3	38.3 ± 1.9	37.1 ± 2.1
<i>S. aureus</i>	49.4 ± 2.3	0 ± 0	32.6 ± 1.6	0 ± 0	0 ± 0	54.2 ± 2.2	44.8 ± 1.8	28.3 ± 1.2	35.4 ± 1.8

Table 4

Antimicrobial activity of the PCL composites after 7 days of immersion in PBS and 100 µm of the supernatant against bacteria. N/B=No bacterial activity present (completely clear).

Bacteria	Zone of inhibition (mm)					
	After Immersion			Supernatant		
	PCL-UiO-66-NH ₂ -CIP	PCL-UiO-66-CIP	PCL-66-NH ₂ -CIP	PCL-UiO-66-NH ₂ -CIP	PCL-UiO-66-CIP	PCL-66-NH ₂ -CIP
<i>E. coli</i>	39.1 ± 2.1	41.5 ± 2.3	34.5 ± 1.7	N/B	N/B	N/B
<i>S. aureus</i>	25.8 ± 2.8	26.7 ± 1.4	26.1 ± 1.2	75.6 ± 3.5	72.6 ± 3.2	73.0 ± 3.1

zone. The supernatant, which contained the released drug, that was extracted after immersion for 7 days was also tested for its antimicrobial activity (Table 4). Against *E. coli*, all three different PCL samples; with CIP and with or without MOFs completely inhibited bacterial growth, leaving the agar growth free and therefore proved the efficiency of the CIP in the release media. Although the zones observed in the case of *S. aureus* were very large, the antimicrobial activity was not as effective against *S. aureus* compared to that observed against *E. coli*, and this was expected as CIP is more active against Gram-negative bacteria.

Table 5 shows a comparison of the antibacterial effect of various CIP formulations compared to other slow-releasing composites of CIP. The results of this study show comparable zones of inhibition to other CIP formulations and the relatively smaller zones of inhibition in the case of the PCL-MOFs-CIP have been attributed to the slower release of CIP from that system, contributing to a more sustainable system for longer term applications.

For further studies, the quantification of the total amount of CIP that was loaded in each MOF and polymer composite will provide a good indication of the longevity of those materials.

4. Conclusions

This study investigated an approach for the controlled and sustained release of ciprofloxacin (CIP), a widely used antibiotic, using porous Zr-based MOF/polymer composites of polycaprolactone. Pristine UiO-66 and UiO-66-NH₂ were successfully synthesized and post-synthetically loaded with CIP followed by their integration into PCL membranes via solvent-casting. All materials were characterised using PXRD, FT-IR, TGA, SEM, gas sorption analysis, UV-Vis analysis for drug release studies, and zone of inhibition - antibacterial studies. Drug release profiles showed that UiO-66-NH₂-CIP presented the highest release in PBS at day-7 with a concentration higher than that released from UiO-66-CIP, but with both materials presenting release of CIP concentrations well above the reported minimum inhibitory concentration (MIC). However, in accelerated aging solutions, release profiles show slight differences between the two MOFs, still well above the MIC. PCL-UiO-66-NH₂-CIP demonstrated the overall slowest release of drug in both PBS and AA, over a period of at least 7 days, at concentrations closer to the MIC. Antimicrobial studies showed that the MOFs exhibited a greater zone of inhibition than their PCL composites, due to slower release from the composite materials. Release studies have also shown pH-dependent release from the composites, with highest release rates at

Table 5

A comparison of the antibacterial effect of different CIP-composite formulations. HS: hyaluronan, LDH: Layered double hydroxide, HA: hydroxyapatite, CS: chitosan.

Ciprofloxacin Composite	Inhibition zones (mm)		reference
	<i>E. coli</i>	<i>S. aureus</i>	
Chitosan/CIP	43.5 ± 0.3	38.1 ± 0.5	Egorov et al. [59]
CIP/HS	–	38 ± 1	Salguero et al. [60]
LDH-CIP/HS	–	33 ± 1	Salguero et al. [60]
HA-CS30-CIP9	22.7 ± 0.3	23.7 ± 0.7	Ait Said et al. [61]
UiO-66-NH ₂ -CIP	50.6 ± 2.3	44.8 ± 1.8	This study
PCL-UiO-66-NH ₂ -CIP	37.1 ± 2.1	35.4 ± 1.8	This study

pH 3 and pH 8.5, owing to the change of the interactions between the MOFs and guest molecules, under various pH. UiO-66-NH₂-CIP showed the greatest antimicrobial effect, within the MOFs, with larger inhibition zones against *E. coli* than *S. aureus*. For the composites, PCL-UiO-66-CIP showed good inhibition of growth against *E. coli* and *S. aureus*. This, combined with the sustained release of CIP by the polymer composites, over a period of at least seven days, demonstrate the successful fabrication of polymer-MOF composites in this study, as a mean for controlled and sustained delivery of ciprofloxacin, and opens scopes for further medical applications of this widely used antimicrobial drug.

Author contributions

SFA: Experiment, materials characterisation, data analysis, manuscript preparation.

LAMM: Data analysis, manuscript preparation.

EHI: Experiment, data analysis, review & editing.

LRT: Terry: Investigation, Formal Analysis, review & editing.

VPT: Supervision, review & editing.

MGK: Supervision, review & editing.

SN: Supervision, review & editing.

Author statement

Following is a list of authors with their contributions highlighted.

Declaration of competing interest

The authors declare that they have no known competing financial interests or personal relationships that could have appeared to influence the work reported in this paper.

Data availability

Data will be made available on request.

Acknowledgements

LAMM and SN acknowledge an Erasmus + exchange studentship. VPT and LRT acknowledge funding via an EPSRC Research Fellowship for VPT [EP/R01650×/1].

Appendix A. Supplementary data

Supplementary data to this article can be found online at <https://doi.org/10.1016/j.jddst.2023.104894>.

References

- [1] EClinicalMedicine, Antimicrobial resistance: a top ten global public health threat, *eClinicalMedicine* 41 (2021), 101221, <https://doi.org/10.1016/j.eclinm.2021.101221>.
- [2] M.E.A. De Kraker, A.J. Stewardson, S. Harbarth, Will 10 million people Die a Year due to antimicrobial resistance by 2050? *PLoS Med.* 13 (2016), e1002184 <https://doi.org/10.1371/journal.pmed.1002184>.
- [3] C.R. Wanda, An overview of the antimicrobial resistance mechanisms of bacteria, *AIMS Microbiol.* 4 (2018) 482–501, <https://doi.org/10.3934/microbiol.2018.3.482>.
- [4] G. Annunziato, Strategies to Overcome antimicrobial resistance (AMR) making use of non-essential target inhibitors: a review, *Int. J. Mol. Sci.* 20 (2019) 5844, <https://doi.org/10.3390/ijms20235844>.
- [5] P. Ramachandran, N. Rachuri, S. Marthia, R. Shakhthivel, A. Gundala, T. Battu, Implications of Overprescription of antibiotics: a cross-sectional study, *J. Pharm. BioAllied Sci.* 11 (2019) 434–437, <https://doi.org/10.4103/jpbs.jpbs.62.19>.
- [6] R. Cantón, M.-I. Morosini, Emergence and spread of antibiotic resistance following exposure to antibiotics, *FEMS Microbiol. Rev.* 35 (2011) 977–991, <https://doi.org/10.1111/j.1574-6976.2011.00295.x>.
- [7] A. Arastehfar, T. Gabaldón, R. Garcia-Rubio, J.D. Jenks, M. Hoenigl, H.J.F. Salzer, M. Ilkit, C. Lass-Flörl, D.S. Perlin, Drug-resistant fungi: an emerging challenge threatening Our limited antifungal armamentarium, *Antibiotics* 9 (2020) 877, <https://doi.org/10.3390/antibiotics9120877>.
- [8] L. Strasfeld, S. Chou, Antiviral drug resistance: mechanisms and clinical implications, *Infect. Dis. Clin.* 24 (2010) 413–437, <https://doi.org/10.1016/j.idc.2010.01.001>.
- [9] P.D. Stapleton, P.W. Taylor, Methicillin resistance in *Staphylococcus aureus*: mechanisms and modulation, *Sci. Adv.* 85 (2002) 57–72, <https://doi.org/10.3184/003685002783238870>.
- [10] R. Smith, J. Coast, The true cost of antimicrobial resistance, *Br. Med. J.* 346 (2013) f1493, <https://doi.org/10.1136/bmj.f1493>.
- [11] L. Sercombe, T. Veerati, F. Moheimani, S.Y. Wu, A.K. Sood, S. Hua, Advances and challenges of liposome assisted drug delivery, *Front. Pharmacol.* 6 (2015), <https://doi.org/10.3389/fphar.2015.00286>.
- [12] S. Kaity, S. Maiti, A. Ghosh, D. Pal, A. Ghosh, S. Banerjee, Microsponges: a novel strategy for drug delivery system, *J. Adv. Pharm. Technol. Research (JAPTR)* 1 (2010) 283–290, <https://doi.org/10.4103/0110-5558.72416>.
- [13] P. Gao, X. Nie, M. Zou, Y. Shi, G. Cheng, Recent advances in materials for extended-release antibiotic delivery system, *J. Antibiot.* 64 (2011) 625–634, <https://doi.org/10.1038/ja.2011.58>.
- [14] S.R. Batten, N.R. Champness, X.-M. Chen, J. Garcia-Martinez, S. Kitagawa, L. Öhrström, M. O'Keefe, M.P. Suh, J. Reedijk, Terminology of metal–organic frameworks and coordination polymers (IUPAC Recommendations 2013), *Pure Appl. Chem.* 85 (2013) 1715–1724, <https://doi.org/10.1351/PAC-REC-12-11-20>.
- [15] M. Karimi, Z. Mehrabadi, M. Farsadrooh, R. Bafkary, H. Derikvand, P. Hayati, K. Mohammadi, Chapter 4 - metal-organic framework, in: M. Ghaedi (Ed.), *Interface Science and Technology*, Elsevier, 2021, pp. 279–387.
- [16] A. Naem, V.P. Ting, U. Hintermair, M. Tian, R. Telford, S. Halim, H. Nowell, M. Holyńska, S.J. Teat, I.J. Scowen, S. Nayak, Mixed-linker approach in designing porous zirconium-based metal–organic frameworks with high hydrogen storage capacity, *Chem Comm* 52 (2016) 7826–7829, <https://doi.org/10.1039/c6cc03787a>.
- [17] D. Yang, B.C. Gates, Catalysis by metal organic frameworks: perspective and suggestions for future research, *ACS Catal.* 9 (2019) 1779–1798, <https://doi.org/10.1021/acscatal.8b04515>.
- [18] L.A.M. Mahmoud, R.A. dos Reis, X. Chen, V.P. Ting, S. Nayak, Metal–organic frameworks as potential agents for extraction and delivery of pesticides and agrochemicals, *ACS Omega* 7 (2022) 45910–45934, <https://doi.org/10.1021/acsomega.2c05978>.
- [19] M. Al Sharabati, R. Sabouni, G.A. Husseini, Biomedical applications of Metal–Organic frameworks for Disease Diagnosis and drug delivery: a review, *Nanomaterials* 12 (2022) 277, <https://doi.org/10.3390/nano12020277>.
- [20] V. Agostoni, R. Anand, S. Monti, S. Hall, G. Maurin, P. Horcajada, C. Serre, K. Bouchemal, R. Gref, Impact of phosphorylation on the encapsulation of nucleoside analogues within porous iron(III) metal–organic framework MIL-100 (Fe) nanoparticles, *J. Mater. Chem. B* 1 (2013) 4231, <https://doi.org/10.1039/c3tb20653j>.
- [21] I. Kritskiy, T. Volkova, T. Sapozhnikova, A. Mazur, P. Tolstoy, I. Terekhova, Methotrexate-loaded metal-organic frameworks on the basis of gamma-cyclodextrin: design, characterization, in vitro and in vivo investigation, *Mater. Sci. Eng., C* 111 (2020).
- [22] N. Ahmad, H.A. Younus, A.H. Chughtai, K. Van Hecke, M. Danish, Z. Gaoke, F. Verpoort, Development of Mixed metal Metal-organic polyhedra networks, colloids, and MOFs and their Pharmacokinetic applications, *Sci. Rep.* 7 (2017) 8, <https://doi.org/10.1038/s41598-017-00733-4>.
- [23] T. Simon-Yarza, T. Baati, F. Neffati, L. Njimi, P. Couvreur, C. Serre, R. Gref, M. F. Najjar, A. Zakhama, P. Horcajada, In vivo behavior of MIL-100 nanoparticles at early times after intravenous administration, *Int. J. Pharm.* 511 (2016) 1042–1047, <https://doi.org/10.1016/j.ijpharm.2016.08.010>.
- [24] N. Singh, S. Quttub, N.M. Khashab, Biocompatibility and biodegradability of metal organic frameworks for biomedical applications, *J. Mater. Chem. B* 9 (2021) 5925–5934, <https://doi.org/10.1039/D1TB01044A>.
- [25] X. Ren, C. Yang, L. Zhang, S. Li, S. Shi, R. Wang, X. Zhang, T. Yue, J. Sun, J. Wang, Copper metal–organic frameworks loaded on chitosan film for the efficient inhibition of bacteria and local infection therapy, *Nanoscale* 11 (2019) 11830–11838, <https://doi.org/10.1039/c9nr03612a>.
- [26] Y. Cai, J.W. Guan, W. Wang, L. Wang, J.Y. Su, L.M. Fang, pH and light-responsive polycaprolactone/curcumin@zif-8 composite films with enhanced antibacterial activity, *J. Food Sci.* 86 (2021) 3550–3562, <https://doi.org/10.1111/1750-3841.15839>.
- [27] P. Rout, Letters to the Editor: topical ciprofloxacin and antibiotic resistance, *Aust. Prescr.* 24 (2001) 27–28, <https://doi.org/10.18773/austprescr.2001.029>.
- [28] D. Bandyopadhyay, Topical antibiotics in dermatology, *Indian J. Dermatol.* 66 (2021) 117–125, https://doi.org/10.4103/ijd.IJD_99_18.
- [29] W. Arif, N.F. Rana, I. Saleem, T. Tanweer, M.J. Khan, S.A. Alshareef, H.M. Sheikh, F.S. Alaryani, M.O. Al-Kattan, H.A. Alatawi, F. Mena, A.Y. Nadeem, Antibacterial activity of Dental composite with ciprofloxacin loaded silver nanoparticles, *Molecules* 27 (2022) 7182, <https://doi.org/10.3390/molecules27217182>.
- [30] S.S. Syed Abdullah, F.A. Faisal Aris, S.N.N. Said Azmi, J.H.S. Anak John, N. N. Khairul Anuar, A.S.F. Mohd Asnawi, Development and evaluation of ciprofloxacin-bacterial cellulose composites produced through in situ incorporation method, *Biotechnol. Rep.* 34 (2022), e00726, <https://doi.org/10.1016/j.btre.2022.e00726>.
- [31] A.O. Basar, S. Castro, S. Torres-Giner, J.M. Lagaron, H. Turkoglu Sasmazel, Novel poly(ϵ -caprolactone)/gelatin wound dressings prepared by emulsion electrospinning with controlled release capacity of Ketoprofen anti-inflammatory drug, *Mater. Sci. Eng. C* 81 (2017) 459–468, <https://doi.org/10.1016/j.msec.2017.08.025>.
- [32] J.H. Cavka, S. Jakobsen, U. Olsbye, N. Guillou, C. Lamberti, S. Bordiga, K. P. Lillerud, A new zirconium inorganic building brick forming metal organic frameworks with exceptional stability, *J. Am. Chem. Soc.* 130 (2008) 13850–13851, <https://doi.org/10.1021/ja8057953>.
- [33] S.M. Chavan, G.C. Shearer, S. Svelle, U. Olsbye, F. Bonino, J. Ethiraj, K.P. Lillerud, S. Bordiga, Synthesis and characterization of amine-functionalized mixed-ligand metal-organic frameworks of UiO-66 topology, *Inorg. Chem.* 53 (2014) 9509–9515, <https://doi.org/10.1021/ic500607a>.
- [34] Y. Wang, W. Lin, S. Yu, X. Huang, X. Lang, Q. He, L. Gao, H. Zhu, J. Chen, A biocompatible Zr-based metal-organic framework UiO-66-PDC as an oral drug carrier for pH-response release, *J. Solid State Chem.* 293 (2021), 121805, <https://doi.org/10.1016/j.jssc.2020.121805>.
- [35] A. Karakecili, B. Topuz, F.S. Ersoy, T. Sahin, A. Gunyakti, T.T. Demirtas, UiO-66 metal-organic framework as a double actor in chitosan scaffolds: antibiotic carrier and osteogenesis promoter, *Biomater. Adv.* 136 (2022), <https://doi.org/10.1016/j.bioadv.2022.212757>.
- [36] J.H. Santos, M.T.J. Quimque, A.P.G. Macabeo, M.J.-A.T. Corpuz, Y.-M. Wang, T.-T. Lu, C.-H. Lin, O.B. Villaflores, Enhanced oral bioavailability of the pharmacologically active lignin magnolol via Zr-based metal organic framework impregnation, *Pharmaceutics* 12 (2020) 437, <https://doi.org/10.3390/pharmaceutics12050437>.
- [37] W. Chen, P. Zhu, Y. Chen, Y. Liu, L. Du, C. Wu, Iodine immobilized UiO-66-NH2 metal-organic framework as an effective antibacterial additive for poly(ϵ -caprolactone), *Polymers* 14 (2022) 283, <https://doi.org/10.3390/polym14020283>.
- [38] M. Nasrabadi, M.A. Ghasemzadeh, M.R. Zand Monfared, The preparation and characterization of UiO-66 metal–organic frameworks for the delivery of the drug ciprofloxacin and an evaluation of their antibacterial activities, *New J. Chem.* 43 (2019) 16033–16040, <https://doi.org/10.1039/c9nj03216a>.
- [39] J. McFarland, The nephelometer: an instrument for estimating the number of bacteria in suspensions used for calculating the OPSONIC index and for vaccines, *J. Am. Med. Assoc. JAMA.* XLIX (1907) 1176, <https://doi.org/10.1001/jama.1907.25320140022001f>.
- [40] M.J. Katz, Z.J. Brown, Y.J. Colon, P.W. Siu, K.A. Scheidt, R.Q. Snurr, J.T. Hupp, O. K. Farha, A facile synthesis of UiO-66, UiO-67 and their derivatives, *Chem. Commun.* 49 (2013) 9449–9451, <https://doi.org/10.1039/c3cc46105j>.
- [41] J. Gandara-Loe, I. Ortuño-Lizarán, L. Fernández-Sánchez, J.L. Alió, N. Cuenca, A. Vega-Estrada, J. Silvestre-Alberro, Metal–organic frameworks as drug delivery platforms for Ocular therapeutics, *ACS Appl. Mater. Interfaces* 11 (2019) 1924–1931, <https://doi.org/10.1021/acami.8b20222>.
- [42] C. Baptista, A. Azagury, H. Shin, C.M. Baker, E. Ly, R. Lee, E. Mathiowitz, The effect of temperature and pressure on polycaprolactone morphology, *Polymer* 191 (2020), 122227, <https://doi.org/10.1016/j.polymer.2020.122227>.
- [43] Y. Cao, H. Zhang, F. Song, T. Huang, J. Q. Zhong, W. Chu, Q. Xu, UiO-66-NH2/GO composite: synthesis, characterization and CO2 adsorption performance, *Materials* 11 (2018) 589, <https://doi.org/10.3390/ma11040589>.
- [44] M. Liu, L. Wang, X. Zheng, Z. Xie, Zirconium-based nanoscale metal–organic framework/poly(ϵ -caprolactone) mixed-matrix membranes as effective antimicrobials, *ACS Appl. Mater. Interfaces* 9 (2017) 41512–41520, <https://doi.org/10.1021/acami.7b15826>.
- [45] M.A. Al-Omar, Ciprofloxacin: analytical profile, in: H.G. Brittain (Ed.), *Profiles of Drug Substances, Excipients and Related Methodology*, Academic Press, 2005, pp. 179–207.
- [46] A. Rivera, L. Valdés, J. Jiménez, I. Pérez, A. Lam, E. Altshuler, L.C. De Ménorval, J. O. Fossum, E.L. Hansen, Z. Rozynek, Smectite as ciprofloxacin delivery system:

- intercalation and temperature-controlled release properties, *Appl. Clay Sci.* 124–125 (2016) 150–156, <https://doi.org/10.1016/j.clay.2016.02.006>.
- [47] M. Unger, C. Vogel, H.W. Siesler, Molecular weight dependence of the thermal degradation of poly(ϵ -caprolactone): a thermogravimetric differential thermal fourier transform infrared spectroscopy study, *Appl. Spectrosc.* 64 (2010) 805–809, <https://doi.org/10.1366/000370210791666309>.
- [48] M. Thommes, K. Kaneko, A. Neimark, J. Olivier, F. Rodriguez-Reinoso, J. Rouquerol, K. Sing, Physisorption of gases, with special reference to the evaluation of surface area and pore size distribution (IUPAC Technical Report), *Pure Appl. Chem.* 87 (2015), <https://doi.org/10.1515/pac-2014-1117>.
- [49] J. Rouquerol, F. Rouquerol, P. Llewellyn, G. Maurin, K.S.W. Sing, *Adsorption by Powders and Porous Solids : Principles, Methodology and Applications*, Elsevier Science & Technology, London, UNITED KINGDOM, 2013.
- [50] L.A.M. Mahmoud, R. Telford, T.C. Livesey, M. Katsikogianni, A.L. Kelly, L.R. Terry, V.P. Ting, S. Nayak, Zirconium-based MOFs and their biodegradable polymer composites for controlled and sustainable delivery of herbicides, *ACS Appl. Bio Mater.* 5 (2022) 3972–3981, <https://doi.org/10.1021/acsabm.2c00499>.
- [51] X. Li, H. Zhang, P. Wang, J. Hou, J. Lu, C.D. Easton, X. Zhang, M.R. Hill, A. W. Thornton, J.Z. Liu, B.D. Freeman, A.J. Hill, L. Jiang, H. Wang, Fast and selective fluoride ion conduction in sub-1-nanometer metal-organic framework channels, *Nat. Commun.* 10 (2019), <https://doi.org/10.1038/s41467-019-10420-9>.
- [52] B.C.L. van der Putten, D. Remondini, G. Pasquini, V.A. Janes, S. Matamoros, C. Schultz, Quantifying the contribution of four resistance mechanisms to ciprofloxacin MIC in *Escherichia coli*: a systematic review, *J. Antimicrob. Chemother.* 74 (2018) 298–310, <https://doi.org/10.1093/jac/dky417>.
- [53] S.S. Al Neyadi, A.G. Al Blooshi, H.L. Nguyen, M.A. Alnaqbi, UiO-66-NH₂ as an effective solid support for quinazoline derivatives for antibacterial agents against Gram-negative bacteria, *New J. Chem.* 45 (2021) 20386–20395, <https://doi.org/10.1039/d1nj03749h>.
- [54] D.P. Hainsworth, J.D. Conklin, J.R. Bierly, D. Ax, P. Ashton, Intravitreal delivery of ciprofloxacin, *J. Ocul. Pharmacol. Therapeut.* 12 (1996) 183–191, <https://doi.org/10.1089/jop.1996.12.183>.
- [55] F. Scaglione, F. Scamazzo, M.M. Arcidiacono, R. Cogo, G.P. Monzani, F. Frascini, Comparative activities of pefloxacin and ciprofloxacin in the treatment of chronic respiratory tract infections, *J. Chemother.* 7 (1995) 140–145, <https://doi.org/10.1179/joc.1995.7.2.140>.
- [56] A.H. Ibrahim, W.A. El-Mehalmey, R.R. Haikal, M.E.A. Safy, M. Amin, H.R. Shatla, S.G. Karakalos, M.H. Alkordi, Tuning the chemical environment within the UiO-66-NH₂ nanocages for charge-dependent contaminant uptake and selectivity, *Inorg. Chem.* 58 (2019) 15078–15087, <https://doi.org/10.1021/acs.inorgchem.9b01611>.
- [57] Y. Huang, N. Dan, W. Dan, W. Zhao, Z. Bai, Y. Chen, C. Yang, Bilayered antimicrobial nanofiber membranes for wound dressings via in situ cross-linking polymerization and electrospinning, *Ind. Eng. Chem. Res.* 57 (2018) 17048–17057, <https://doi.org/10.1021/acs.iecr.8b03122>.
- [58] M. Mozafari, S. Kargozar, G.T. de Santiago, M.R. Mohammadi, P.B. Milan, M. Foroutan Koudehi, B. Aghabarari, M.R. Nourani, Synthesis and characterisation of highly interconnected porous poly(ϵ -caprolactone)-collagen scaffolds: a therapeutic design to facilitate tendon regeneration, *Mater. Technol.* 33 (2018) 29–37, <https://doi.org/10.1080/10667857.2017.1379678>.
- [59] A.R. Egorov, M.N. Kurasova, O. Khubiev, N.A. Bogdanov, A.G. Tskhovrebov, A. A. Kirichuk, V.N. Khrustalev, V.V. Rubanik, V.V. Rubanik, A.S. Kritchenkov, Ciprofloxacin chitosan conjugate: combined antibacterial effect and low toxicity, *Mendelev Commun.* 32 (2022) 774–776, <https://doi.org/10.1016/j.mencom.2022.11.022>.
- [60] Y. Salguero, L. Valenti, R. Rojas, M.C. García, Ciprofloxacin-intercalated layered double hydroxide-in-hybrid films as composite dressings for controlled antimicrobial topical delivery, *Mater. Sci. Eng. C* 111 (2020), 110859, <https://doi.org/10.1016/j.msec.2020.110859>.
- [61] H. Ait Said, H. Noukrati, H. Ben youcef, I. Mahdi, H. Oudadesse, A. Barroug, In situ precipitated hydroxyapatite-chitosan composite loaded with ciprofloxacin: formulation, mechanical, in vitro antibiotic uptake, release, and antibacterial properties, *Mater. Chem. Phys.* 294 (2023), 127008, <https://doi.org/10.1016/j.matchemphys.2022.127008>.